Supplementary Material

For the manuscript: “Thermodynamic Advantage of Transient Wave Dynamics in Hierarchical Decision Architectures. Coherent Resonant Netting (CRN) via an Open-System Formalism.”

Corresponding author: Oleg Dolgikh (hanlon@occam.world) ORCID: 0009-0008-0159-1718

This document consolidates supplementary notes referenced in the main text (S1–S6). Numerical artifacts and code are provided in the Supplementary Simulation Suite (R12-CROWN) archived on Zenodo (concept DOI: 10.5281/zenodo.18338260; version used here: 10.5281/zenodo.18338261).

Supplementary Note S1: Supplementary Simulation Suite (R12-CROWN) and Reproducibility

The Supplementary Simulation Suite (R12-CROWN) contains a lightweight, self-contained implementation of the GKSL transport model on graphs, the analysis routines used to compute the Liouvillian gap and window widths, and the figure-generation scripts used to reproduce the computational results in the manuscript.

Contents (see README.md in the archive):

- qrn_core.py — GKSL (Lindblad) engine on a graph with node-local dephasing and an explicit sink state $|s\rangle$.
- qrn_analysis.py — spectral-gap sweeps, robustness window widths, threshold-sink robustness, checkpoint validation.
- qrn_viz.py — plotting helpers (PNG generation).
- run_all.py — regenerates the full figure and CSV bundle into ./outputs/.
- compare_baselines.py — baseline CRN vs classical random walk (CRW) control used in Supplementary Note S6.
- compare_baselines_barrier.py — barrier-limited classical baseline control used in Supplementary Note S6.
- validate_checkpoints.py — PASS/FAIL validation for key numerical checkpoints (checkpoints.yaml).
- MANIFEST.md — file manifest and integrity hashes for key outputs.

Quick start (from inside the R12-CROWN folder):

- python run_all.py

Outputs are written to ./outputs/. The archive also includes a pre-generated outputs folder for convenience; rerunning the suite regenerates those files from source.

Quick reproduction (large-N, N=1000; Figures 3, 5, and 6) (from inside the R12-CROWN-LargeN-N1000 folder):

- python run_largeN_stress_test.py --config config_largeN.json

Outputs are written to ./outputs/ and include the combined figure bundle (largeN_stress_test.png) and CSV artifacts (largeN_kappa_sweep.csv, largeN_energy_sweep.csv).

Supplementary Note S2: Physical Grounding and the Feasibility Checkpoint

Candidate substrates for mesoscopic wave dynamics.

The CRN framework is compatible with multiple classical wave carriers, but it does require phase/amplitude variables and interference effects on 10–100 ms timescales. Three plausible biological candidates are:

- Dendritic integration fields (subthreshold interference prior to somatic spiking).
- Gamma-band phase coupling ("communication through coherence") as an effective complex-coupling medium.
- Neural field modes (damped cortical waves; mean-field propagation with delays) abstracted into a graph of dominant modes.

In the main text we use a dimensionless GKSL generator with rates (γ, κ, η) expressed in a common unit system (we set $\hbar = 1$ and measure time in inverse-rate units). To connect model timescales to physiology, one needs a single empirical anchor to set the physical time unit; all other model times follow by proportionality.

Recommended calibration procedure:

1. Choose an experimentally accessible cycle time. In reset-limited decision circuits, the most direct anchor is the mean recovery/reset timescale τ_{reset} (e.g., inter-bout interval, refractory recovery of the relevant decision module, or a measurable "cooldown" time until the next decision becomes possible).
2. Map the model's reset-limited act rate $f_{fix} \approx 1/\tau_{reset}$ (main text, Eq. (4)) to the empirical act rate. This sets the conversion between model time units and milliseconds.
3. Convert the model transport/pre-selection timescale (τ_{trans} or g(κ)^{-1}) to physical units. The feasibility checkpoint is that the physical substrate must maintain phase memory over a comparable interval: $\tau_{\varphi} \gtrsim \tau_{trans}$ (order-of-magnitude).

Combined with the energy checkpoint χ in Supplementary Note S4, this "phase-budget" criterion (requiring τ_φ ≳ τ_trans) provides a simple filter: substrates that cannot maintain phase memory over the required transport timescale, or that would require $\chi \gtrsim 0.1$ to do so, are effectively excluded as candidates for the CRN wave layer.

Operational guidance on what to measure/estimate:

Quantity	Meaning in CRN	Empirical proxy (examples)
τ_{reset}	Reset-limited cycle time; sets the act rate f_{fix}	Inter-decision interval; recovery from synaptic depression; circuit "cooldown" dynamics
τ_{trans}	Wave episode / transport time on the active subgraph	Latency of subthreshold integration; dendritic plateau/burst initiation window; LFP phase persistence (if applicable)
κ	Effective dephasing/noise rate that interpolates between interference and overdamped diffusion	Temperature/anesthetic modulation; variability of membrane potential; channel noise proxies
γ	Effective coupling/transport strength on the hypothesis graph	Functional connectivity within the engaged microcircuit; effective coupling inferred from dynamics

We emphasize that this is a calibration strategy, not a claim that the model parameters are uniquely identifiable from behavior alone. Parameter non-identifiability is explicitly discussed as a limitation in the main text (Section 7.5).

Interpretation of ρ (state descriptor) as an effective coherency matrix

This note makes explicit the interpretation of the state descriptor ρ(t) used in the main text's GKSL/Lindblad formulation. We do not treat ρ as a microscopic quantum density matrix of neural tissue; rather, it is a compact mesoscopic descriptor of wave-like population variables on the active hypothesis graph.

Let a_j(t) ∈ ℂ denote a band-limited oscillatory amplitude proxy at node j (e.g., a dendritic field mode, an LFP/MEG phasor, or a synchronization variable). Define ρ_{jk}(t) := ⟨ a_j(t) a_k(t)^* ⟩, where ⟨·⟩ denotes averaging over fast microscopic fluctuations/ensembles.

Diagonal elements ρ_{jj} track population/intensity (hypothesis weight) and can be mapped to power/envelope measures. Off-diagonal elements summarize phase relations/coherence between nodes and are the degrees of freedom that enable constructive/destructive interference on the graph.

Under this interpretation, Eq. (3) separates three functional processes: coherent transport driven by H_net (phase-sensitive redistribution on the hypothesis graph), effective dephasing/noise at rate κ that attenuates off-diagonals, and an irreversible sink/readout channel (η) representing Stage-II fixation/commitment. The formalism is therefore compatible with classical wave substrates; experimentally, the focus is on regime inference (κ*, W_κ) and stage-dissociation signatures rather than microscopic ontology.

Functional mapping of terms (at the level of effective dynamics):

- -i[H_net, ρ]: coherent graph transport and interference ("netting").
- κ-dissipator(s): dephasing/noise that interpolates between interference and overdamped diffusion.
- η-sink term: thresholded fixation/readout proxy (irreversible commitment).

Supplementary Note S3: Spectral Structure and Mode Separation (Operational "Resonance")

In the main text (Section 4.3) we use the term "resonant" in an operational sense: the wave layer is effective when the dynamics exhibits a structured spectrum of modes with separable timescales. Practically, this means that (i) there exist transport-relevant modes whose phase relations persist over the traversal time τ_trans, while (ii) a larger set of components decays rapidly and can be treated as transient or noise-driven.

Within the GKSL framework, this structure is reflected in the spectrum of the Liouvillian generator $\mathscr{L}$. The Liouvillian gap g provides the leading relaxation rate, but "mode separation" refers more generally to the presence of a subset of slow modes (small |Re(λ)|) separated from fast-decaying modes by a spectral shoulder. When such separation is present, Stage I can act as a selective pre-filter: interference suppresses inconsistent paths before the readout/nonlinearity amplifies a discrete winner.

Operational diagnostics (suggested):

- Plot the empirical distribution of Re(λ_j) of $\mathscr{L}$ for representative (γ, κ, η) and identify whether a clear slow/fast partition exists (e.g., a gap or shoulder in Re(λ)).
- Report how the slow-mode set and g(κ) shift with κ and with connectivity-like perturbations (γ), and whether the ENAQT-like / noise-assisted transport (NAT) optimum coincides with maximal separation (fast decay of spurious components with preserved transport coherence).
- If mode separation is absent (all decay rates form a single broad band), the "resonant" label should be de-emphasized and the architecture reduces to generic noise-tuned diffusion. In that case, any observed intermediate-noise optimum would be better interpreted through classical stochastic-resonance or diffusion-with-threshold models rather than as evidence for a distinct CRN-like pre-selection layer.

Supplementary Note S4: Payoff Maps for the Energy Checkpoint

Section 6.3 defines an operational "energy checkpoint" in terms of the dimensionless ratio $\chi := E_{tax}/E_{comm}$ (main text, Eq. (6)). Here χ denotes the checkpoint ratio; the open-system state descriptor in the main text is written as $\rho(t)$. Here E_{tax} is the mean wave-layer tax per decision act and E_{comm} is the spike-equivalent cost of one long-range communication event.

- $\chi \lesssim 10^{-2}$ — strong energetic advantage in the communication-dominant regime (wave-layer tax is only a few percent of one spike-equivalent event).
- $10^{-2} \lesssim \chi \lesssim 10^{-1}$ — transitional band where advantage depends on task structure and implementation details.
- $\chi \gtrsim 10^{-1}$ — "red-line" region where the wave layer becomes thermodynamically disadvantageous and classical baselines may be competitive.

The R12-CROWN archive includes numerical payoff artifacts and a reset-sweep example that computes and the checkpoint ratio over (see outputs/energy_sweep.csv and outputs/energy_regime.png). These artifacts are intended as templates: the same logic applies to other control sweeps (e.g., over , , topology) provided that and can be estimated for the substrate under study.

S4.1 Worked order-of-magnitude example (illustrative heuristic)

This subsection gives a compact numerical sanity check for the checkpoint ratio χ := E_tax/E_comm. Let P_tax denote the incremental power required to keep the Stage I wave regime available during an act, beyond the baseline cost of the classical fixation/broadcast circuitry. The per-act tax is then E_tax = P_tax/f_fix (reset-limited f_fix ≈ 1/τ_reset). If a candidate implementation is dendritic field dynamics in a small L5 microcolumn (order 10^2 neurons), a conservative heuristic is to benchmark E_tax against one spike-equivalent broadcast event E_comm: if E_tax ≈ (0.02-0.05)·E_comm, then χ ≈ 0.02-0.05 (safe band). This is not a claim that the wave layer is uniquely dendritic, nor a precise biophysical estimate; it is an illustrative scale-setting example to make χ operational and falsifiable.

S4.2 From observables to a conservative upper bound on χ

1) Measure f_fix and confirm the reset-limited regime. Operationally, define one act as the interval between two successive fixation/broadcast events, and estimate f_fix from inter-event intervals. Check that f_fix is primarily constrained by τ_reset rather than by the Stage I transport time τ_trans.

2) Bound E_comm (spike-equivalent broadcast energy). Use spike/burst counts per act together with literature-based energy-per-spike estimates, or a differential metabolic readout in a condition where broadcast events are evoked/isolated at matched rates. The goal is an order-of-magnitude bracket, not a single precise value.

3) Bound P_tax (incremental wave-layer maintenance power). Use a differential design that holds fixation/broadcast approximately constant while varying a wave-layer proxy (or suppresses broadcast while preserving subthreshold dynamics), and measure the incremental metabolic load (e.g., NADH/FAD fluorescence, CBF/CMRO2, oxygen/glucose consumption) attributable to the pre-selection regime.

4) Compute an upper bound χ_upper = (P_tax / f_fix) / E_comm and report it with uncertainty. If conservative bounds place χ in the red-line band (χ ≳ 0.1) under realistic operating conditions, the energy-advantage component of CRN is effectively falsified even if NAT-like behavioral signatures are present.

S4.3 Indirect Q4 test via scaling with task complexity (N_active)

A simple indirect marker of Q4 is scaling: as task complexity increases (larger recruited active subgraph N_active), the incremental metabolic load attributable to the Stage I regime (P_tax or E_tax per act) should grow sublinearly relative to throughput or to N_active. An approximately linear scaling over the operating range would imply that maintenance/control losses cancel the putative savings and would push χ toward (or above) the red-line region.

S4.5 Integration with Main-Text Claims

The checkpoint variable χ is used in the main text as a falsifiable intermediate claim: if $\chi := E_{tax} / E_{comm}$ is < 0.1 in realistic parameter ranges, then pre-selection can be energetically worthwhile; if $\chi \gtrsim 0.1$, CRN may still be mechanistically correct, but its energy-economy claim would fail.

Summary: Interpreting χ and the energy checkpoint.

- $\chi < 0.01$: Strong support for CRN's thermodynamic advantage (wave-layer tax is negligible).
- $0.01 < \chi < 0.1$: Moderate support; advantage is task-dependent and sensitive to implementation details.
- $\chi \gtrsim 0.1$: Falsifies the strong energy-advantage claim (CRN may still operate, but without net savings).

S4.6 Limitations and Caveats

1. Parameter non-identifiability: In practice, P_tax, f_fix, and E_comm may be difficult to estimate independently. Use conservative upper bounds.
2. Substrate specificity: The definition of E_comm depends on what is taken as the baseline communication event. The checkpoint is comparative, not absolute.
3. Context dependence: In some systems, the Stage I wave layer may not be purely "idle"; it may also perform useful subthreshold computation. In such cases, P_tax is partially offset by computation and χ can overestimate overhead.
4. Indirect measurements: χ is often inferred indirectly from metabolic proxies (CBF, CMRO2, glucose uptake). Such proxies have limited resolution and may include non-decision energy contributions.
5. Temporal dynamics: This treatment assumes quasi-steady-state conditions. In rapid transient tasks, power/energy partitioning may vary across time and local circuit state.

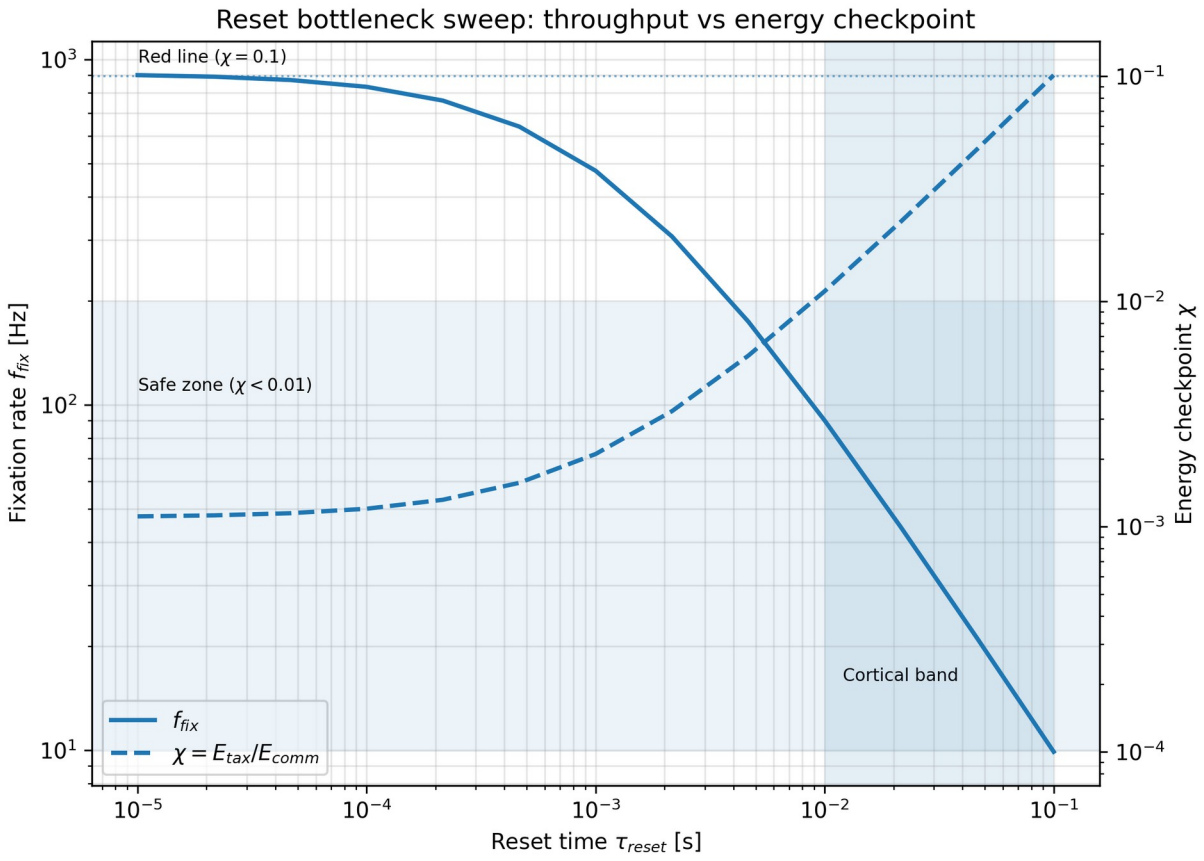

Supplementary Figure S4-1: Example checkpoint sweep from R12-CROWN (energy_regime.png).
Illustrative sweep showing the dependence of fixation/act rate and the checkpoint ratio on the reset timescale in a reset-limited regime. The plot highlights the safe region (χ well below the red-line) and the transition as τ_{reset} increases.

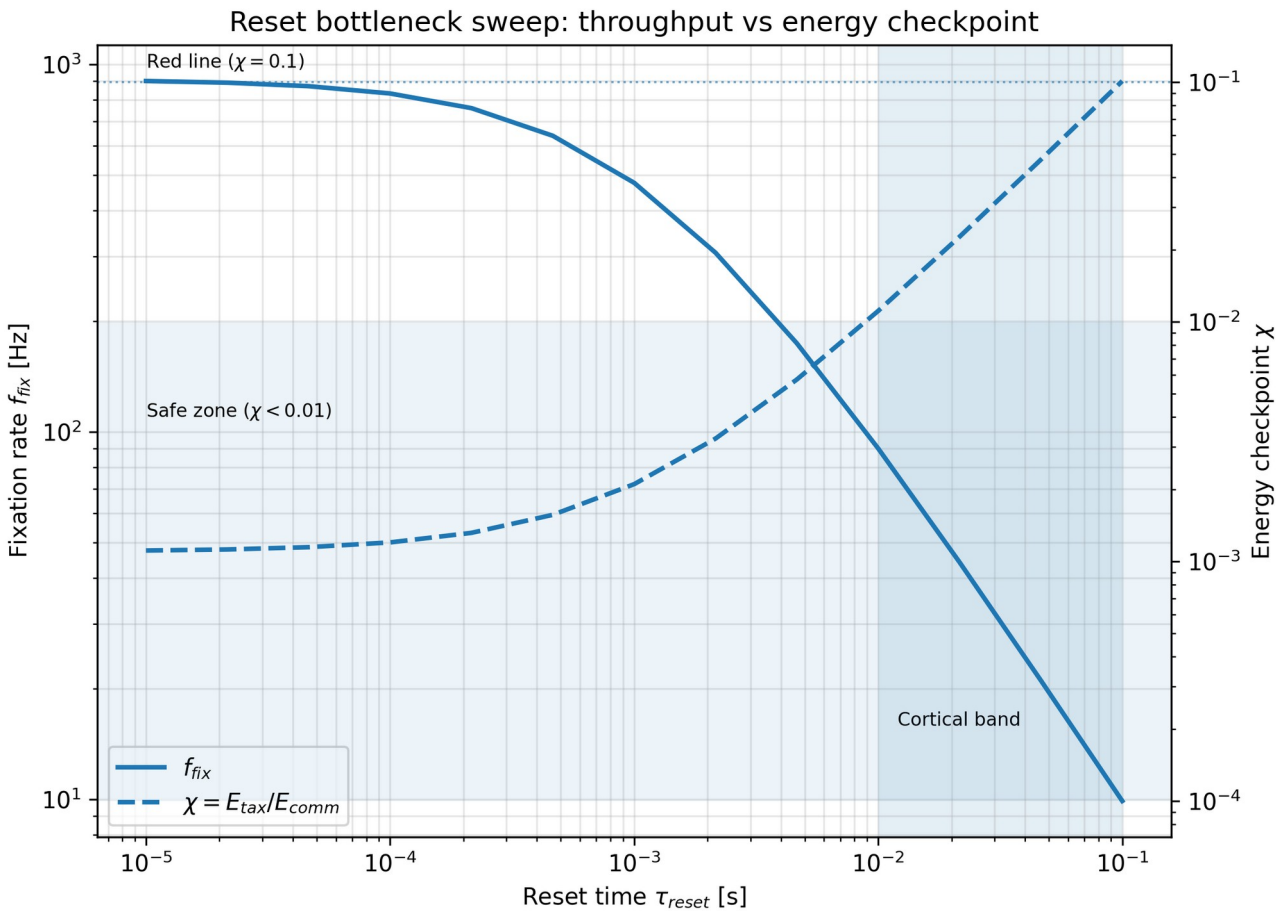

Supplementary Note S5: Extended Drosophila Protocol for P1–P3 and P5

This note expands the brief protocol sketch in Section 7.2. The goal is not to prove a microscopic substrate, but to test architecture-level predictions that distinguish (i) reset-limited control of act rate from (ii) noise/dephasing control of an ENAQT-like / noise-assisted transport (NAT) optimum.

Core logic (2×2 dissociation):

- Manipulate κ-proxy (noise/dephasing) while keeping τ_reset-proxy approximately fixed. Prediction: a non-monotonic ENAQT-like / noise-assisted transport (NAT) curve in latency/accuracy with an intermediate-noise optimum (P1), and a broad functional width (P2).
- Manipulate τ_reset-proxy (reset dynamics) while keeping κ-proxy approximately fixed. Prediction: near-linear scaling of maximal act/decision rate f_fix with 1/τ_reset and minimal shift of κ_opt (P3).

Candidate handles (examples; specific choices depend on the behavioral assay and circuit):

- Reset proxy (τ_{reset}): temperature-sensitive shibire (shi^{ts1}) to reversibly impair synaptic vesicle recycling and alter recovery dynamics in targeted circuits (Kitamoto, 2001). Alternative reset handles include manipulations that change synaptic depression/recovery or circuit-level inhibition/excitation balance that controls “cooldown” time.

- Noise proxy (κ): mild anesthetic modulation at fixed temperature (to perturb synaptic release reliability and membrane noise statistics), channel-noise manipulations, or controlled sensory noise in the stimulus stream (when the assay allows separating internal from external noise).
- Readout/throughput: decision latency distributions, accuracy/choice fraction, and maximal repetition rate under paced or self-paced conditions. Where feasible, include physiological proxies (e.g., calcium imaging of dendritic events, metabolic reporters) to constrain parameter identifiability.

Analysis outputs and falsification criteria:

- Estimate an ENAQT-like / noise-assisted transport (NAT) curve by plotting a decision metric (latency, accuracy, or a combined throughput measure) versus -proxy. Falsification of P1: monotonic improvement as decreases, or an optimum explainable by a purely rate-based stochastic resonance lacking a spectral/dynamical counterpart.
- Estimate window width from the κ–metric curve (e.g., FWHM on a log κ axis) as a robustness diagnostic (P2).
- Test dissociation by fitting separate effects: κ-proxy should primarily reshape the curve (produce a peak), whereas τ_{reset}-proxy should primarily rescale achievable act rate without producing the same non-monotonic shape (P3).
- Optionally, search for fine-structure (Figure 8 in main text) only after establishing coarse signatures. Fine-structure is an optional, high-resolution marker and is explicitly not required as a success criterion in the manuscript's falsification logic.

Practical note on confounds: temperature changes affect multiple processes simultaneously. When temperature is used as a reset handle (e.g., shi^{ts1}), κ-proxy manipulations should preferentially rely on non-temperature perturbations (e.g., anesthetics at constant temperature) or on within-temperature comparisons that control for baseline Arrhenius/Q10 effects.

Supplementary Table S5-1: Falsification Matrix for CRN (P1–P6 aligned with main text)

Prediction	Behavior (example)	Physiology (example)	Falsified if…
P1: Non-monotonic noise optimum (ENAQT/NAT)	Peak performance (latency/accuracy/throughput) at κ_opt	Phase-sensitive spectral/relaxation proxy peaks at κ_opt (e.g., g(κ) max)	Monotonic behavior across κ; no spectral peak or misaligned optima
P2: Robustness window W_κ	Near-optimal zone spans ≥0.3 decades on log10(κ) (e.g., ≥80% of peak)	W_κ (from g(κ) or behavioral curve) is not ultra-narrow	W_κ ≪ 0.1 decades (fine-tuned/fragile peak)
P3: Reset/noise orthogonality	τ_reset-like manipulations rescale max act rate (f_fix≈1/τ_reset) without shifting κ_opt	Noise-like vs reset-like manipulations dissociate in Stage I vs Stage II markers	κ_opt shifts strongly with τ_reset, or both knobs produce indistinguishable effects
P4: Energy checkpoint χ = E_tax/E_comm	Energetic viability requires $\chi \ll 1$ (red-line at $\chi \gtrsim 0.1$)	Estimated/bounded χ safely below 0.1 under realistic operating conditions	$\chi \gtrsim 0.1$ (wave-layer tax negates advantage)
P5: Anesthesia shifts	Anesthetic dose moves system away from κ_opt; predictable shift in inferred κ_opt/window	Spectral/relaxation proxies shift consistently with increased effective κ or weakened coupling	Robust behavioral anesthesia effect with no shift (or opposite shift) in κ_opt/g(κ) markers
P6: Mammalian/human	Stage I non-monotonic vs	β–γ coherence/PLV	Both stages show the

two-stage dissociation	κ; Stage II monotonic degradation with κ	peaks near κ_opt; P300/RP latencies increase with κ	same monotonic κ-dependence (no dissociation)

S5.2 Extension to Mammals and Humans (P6 Protocol)

Rationale and Scope

While CRN's core predictions (P1–P5) are most efficiently tested in genetically tractable invertebrate models (e.g., Drosophila), the central architectural claim—a two-stage, noise-sensitive pre-selection layer followed by a deterministic fixation layer—should generalize to vertebrates if the mechanism is conserved. P6 specifies an experimentally testable dissociation signature that distinguishes Stage I (pre-selection) from Stage II (fixation) via contrasting noise dependence.

- Stage I (pre-selection): non-monotonic efficiency vs the effective dephasing/noise rate κ (ENAQT-like optimum).
- Stage II (fixation): monotonically degraded commitment latency/reliability with increasing noise.

This dissociation is the key signature that rules out simpler alternatives (e.g., a single diffusive threshold process or uniform stochastic resonance) and makes P6 falsifiable in mammals/humans.

Neurophysiological Signatures and Measurement Strategy

Stage I markers (pre-selection): beta-gamma coherence and phase locking

In CRN, Stage I manifests as a transient episode of phase-sensitive interference on a distributed neural graph. In mammalian circuits, this corresponds most directly to transient, decision-locked coherence/phase-locking across relevant cortical–subcortical nodes.

- **Regional LFP/EEG coherence (beta-gamma band, 15–80 Hz):** Compute pairwise coherence between task-relevant regions (e.g., PFC–ACC, PFC–parietal). Coherence can be estimated as $C(f) = |S_{xy}(f)| / \sqrt{S_{xx}(f) \cdot S_{yy}(f)}$. Expected: a non-monotonic peak at an intermediate κ (κ_opt), with suppression at both low-κ (ballistic trapping) and high-κ (overdamped diffusion).
- **Phase-locking value (PLV) or weighted phase lag index (wPLI):** $PLV = |\langle \exp(i(\varphi_x - \varphi_y)) \rangle|$ provides a phase-based measure less sensitive to amplitude scaling; wPLI is more robust to volume conduction. Expected: a non-monotonic peak at κ_opt in the pre-decision window.
- **Spectral power (alpha/beta bands) in the pre-decision window:** Power changes are less specific than coherence/PLV, but an intermediate-noise enhancement in pre-selection-related bands can support Stage I engagement. Caveat: treat power effects as secondary, and prioritize phase-based metrics.
- **Temporal dynamics (decision-locked transient):** Stage I markers should exhibit a transient, decision-locked peak (typically ~100–300 ms before fixation/response), consistent with a short "netting" episode prior to readout.

Stage II markers (fixation): P300, readiness potential, and latency

Stage II is a discrete thresholded readout that commits the selected hypothesis via an effectively irreversible transition. Behaviorally and electrophysiologically, this is expected to yield canonical commitment/decision markers that degrade monotonically with increasing noise.

- **P300 latency (and amplitude):** P300 latency is expected to increase monotonically with κ (no intermediate optimum), reflecting slowed commitment/fixation. Amplitude may show task-dependent non-monotonicity, so latency is the primary fixation-timescale readout.

- **Readiness potential (RP/Bereitschaftspotential) latency or slope:** In self-paced or action-selection tasks, RP timing/slope should degrade monotonically with κ. Use EMG and response-locked averaging to dissociate decision latency from motor execution latency.
- **Reaction time (RT) distribution and accuracy:** Mean RT is expected to increase monotonically with κ, while accuracy can show an intermediate optimum due to Stage I. A key dissociation is RT monotonicity coexisting with a non-monotonic accuracy/coherence peak.

Experimental Design and Noise Manipulations

Core 2×2 dissociation logic: apply two orthogonal manipulations—(i) a κ-proxy that modulates effective noise/dephasing, and (ii) a τ_reset-proxy that modulates act rate/throughput—then test whether Stage I and Stage II markers respond differently.

Manipulation 1: Noise/dephasing proxy (κ)

- **Transcranial random noise stimulation (tRNS):** Increases cortical excitability and injects broadband noise. Expected: move along the κ axis; moderate tRNS can enhance Stage I coherence (approaching κ_opt), while excessive tRNS degrades both stages.
- **Acute stress induction:** Elevates neuromodulators/cortisol and increases network variability. Expected: right-shift of κ_opt and reduced Stage I peak amplitude due to increased baseline noise.
- **Environmental or stimulus-based noise:** Add controlled sensory noise (e.g., visual jitter, auditory masking) to increase uncertainty. Expected: similar non-monotonic Stage I effects; ensure sensory confounds are separated from neural noise.
- **Pharmacological noise modulation:** Mild sedatives (e.g., benzodiazepines) reduce synaptic variability; stimulants can enhance synaptic noise. Expected: BZD shifts leftward on κ (κ_opt at lower external noise), stimulants shift rightward. Caveat: system-wide effects are substantial; best implemented in animal models with careful controls.

Manipulation 2: Reset/refractoriness proxy (τ_reset)

- **Inter-trial interval adjustment:** Impose variable delays between trials to change recovery/reset time. Predicted to rescale throughput $f_{fix} \approx 1/\tau_{reset}$ without shifting κ_opt.
- **Decision pacing:** Compare self-paced versus forced-paced regimes. Forced pacing can saturate reset dynamics and push the system into a reset-limited throughput regime.
- **Circuit-level inhibition/excitation balance (animal models):** Manipulate inhibitory tone to slow network reset (indirect τ_reset proxy). Expected: decreased throughput (longer τ_reset) but approximately invariant κ_opt; use to separate reset effects from noise tuning.

Behavioral Assays and Decision Contexts

Recommended decision paradigms (choose assays where decision onset and fixation are temporally separable, and where trial structure supports EEG/MEG time-locking):

- **Perceptual discrimination:** Two-alternative forced-choice (2AFC) tasks (e.g., random-dot motion, tone discrimination). Measure accuracy and RT; apply sensory noise and/or tRNS; compute decision-locked coherence.
- **Value-based choice:** Choices between gambles/delays engaging PFC–ACC–striatal circuits. Noise manipulations via stress, tRNS, or pharmacology (animal). Evaluate dissociation between pre-choice coherence and post-choice fixation markers.
- **Motor action selection:** Target selection (reach/saccade) or Go/No-Go variants. Enables readiness potential and EMG-based separation of decision vs motor components.

- **Evidence accumulation under uncertainty:** Sequential evidence tasks (drift-diffusion context) allow explicit modeling of decision time vs non-decision time, and provide a strong control against single-stage alternatives.

Predicted Dissociation Patterns

Canonical CRN signature: non-monotonic Stage I (pre-selection) vs monotonic Stage II (fixation) as κ increases.

Noise level (κ)	Stage I (pre-selection)	Stage II (fixation)	Behavioral expectation
Low (ballistic)	Coherent trapping; inefficient filtering	Fast threshold crossing; low noise-driven latency	Fast RT; may be brittle under ambiguity
Intermediate (κ_opt)	Maximum filtering/transfer efficiency (ENAQT-like optimum)	Moderate latency; reliable commitment	Peak performance (accuracy/throughput)
High (overdamped)	Diffusive; loss of coherent selectivity	Slow, noisy threshold crossing; higher error	Slow RT; increased variance; degraded accuracy

Dissociation test (operational): plot Stage I and Stage II metrics as functions of κ.

- **Pre-selection fidelity:** Expected: inverted-U with a peak near κ_opt (use accuracy on controlled trials and/or pre-decision coherence/PLV magnitude).
- **Behavioral fixation latency (mean RT):** Expected: monotonically increasing with κ (no intermediate optimum).
- **Decision-locked coherence before commitment:** Expected: non-monotonic peak near κ_opt in a pre-response window (e.g., 200–300 ms before response).
- **Neural fixation latency (P300 latency / RP timing):** Expected: monotonically increasing with κ (commitment slows with noise).

Falsification criterion: if all markers show monotonic degradation with κ, or if all markers show non-monotonic behavior with a shared optimum, then the two-stage Stage I/Stage II dissociation predicted by CRN is not supported.

Measurement Protocol and Analysis

Use a within-subject factorial design with multiple κ-proxy levels (e.g., 3–5) crossed with ≥2 τ_reset-proxy levels. Randomize condition order and include sham/control conditions for stimulation and stress manipulations.

Primary analysis outputs:

- Stage I: coherence/PLV time-frequency maps; peak magnitude and peak location on the κ axis; robustness window width W_κ (e.g., FWHM on log10 κ).
- Stage II: P300 latency (and/or RP timing), RT distribution moments (mean, variance), and diffusion-model (DDM) decomposition of decision vs non-decision time.
- Dissociation statistics: regression/ANOVA with a quadratic term for Stage I markers versus a linear term for Stage II markers; test for Stage×κ interaction.

A minimal confirmatory test is: Stage I markers show a significant inverted-U (quadratic) dependence on κ, while Stage II latency markers show a significant monotonic trend without an intermediate optimum.

Expected Results and Interpretations

- **Success scenario (strong CRN support):** Stage I coherence/accuracy peaks at intermediate κ (κ_opt), while Stage II P300 latency and RT degrade monotonically with κ. Stage I and Stage II metrics dissociate.
- **Partial support (mixed signature):** Stage I shows non-monotonicity but Stage II also shows a weak optimum. This can indicate confounds (arousal, sensory SNR changes) or incomplete stage separation; apply controls and DDM decomposition.
- **Negative outcome (P6 falsification):** Both Stage I and Stage II markers degrade monotonically with κ. This pattern supports a single-stage diffusive threshold model (or uniform noise impairment) rather than CRN's two-stage dissociation.

Practical Implementation Notes

- Feasibility: high-density EEG/MEG with response-locked time-frequency analysis is sufficient for Stage I/II dissociation; invasive LFPs improve spatial specificity (animal models).
- Design: prioritize within-subject designs to reduce inter-individual variability in κ_opt and W_κ; pre-register the primary dissociation tests (quadratic vs linear effects).
- Controls: include sham stimulation, arousal covariates (pupil dilation), and motor controls (EMG) to separate decision from output noise.

Population-Specific Variants

- **Age:** Compare younger vs older cohorts: predicted right-shift of κ_opt and reduced robustness window W_κ due to increased baseline neural noise.
- **Anxiety / high-arousal traits:** Potential left-shift of κ_opt and reduced W_κ (fragile tuning); require explicit arousal controls.
- **Attention-deficit phenotypes:** Potential right-shift of κ_opt and increased RT variance even near κ_opt; interpret alongside DDM fits.
- **Animal models (rodent/primate):** Enable direct PFC/ACC LFP coherence and pharmacological κ / τ_reset manipulations; map LFP signatures to human EEG/MEG markers.

Alternative Mechanistic Explanations and Controls

Controls for Confounding Interpretations

- **Stochastic resonance (SR):** SR alternative predicts noise enhances detection/SNR uniformly across pre- and post-decision stages. Control: decompose RT into decision time vs non-decision time (DDM); Stage I-specific non-monotonicity in decision time supports CRN.
- **Arousal/attention effects:** tRNS or stress may globally increase arousal and speed RT. Control: measure pupil dilation; include arousal as a covariate; use sham tRNS and counterbalanced condition order.
- **Motor/output noise:** High noise may degrade motor execution (slower/more variable button presses). Control: measure EMG and use RP timing to dissociate decision latency from motor execution latency; apply RT mixture models.

Mechanistic Alternatives to Rule Out

- **Pure diffusion + threshold:** Predicts RT increases monotonically with noise (consistent with Stage II), but Stage I coherence should not show an intermediate peak. Absence of Stage I peak disfavors CRN.
- **Single-layer noise-tuned resonance:** Would predict uniform noise dependence across all markers; falsified by a Stage I vs Stage II dissociation.
- **Predictive coding with prediction errors:** May explain some post-decision error signals, but does not parsimoniously predict Stage I transient coherence with an ENAQT-like optimum.

Supplementary Table S5.2-1: Falsification Matrix for P6

Prediction	Mammalian marker	Expected noise dependence	Falsified if…
P6a	β-γ LFP/EEG coherence (15–80 Hz)	Non-monotonic peak at κ_opt	Monotonic across all κ
P6c	P300 latency	Monotonically increases with κ	Shows intermediate optimum
P6d	Readiness potential (RP) latency	Monotonically increases with κ	Shows non-monotonic pattern
P6e	Reaction time distribution	Monotonic degradation (variance ↑)	Shows U-shaped curve
P6 dissociation	Stage I vs II markers anti-correlate	Coherence peaks where RT is fast	Coherence and RT both monotonic

Supplementary Note S6: Baseline comparison against classical random walk (CRW)

This note supports the main-text discussion in Section 7.3 (Biological Implementation and Distinction from Classical Models). This note provides a minimal "baseline control" addressing the classical mimicry concern: an ENAQT-like / noise-assisted transport (NAT) optimum in CRN should not be confused with generic stochastic resonance or a purely diffusive transport process. We therefore compare CRN's GKSL-based wave dynamics against a continuous-time classical random walk (CRW) on the same graph topology, using the same sink (absorption) rate at the target node. The goal is not to establish a quantitative speedup, but to illustrate qualitative phenomena—interference trapping and its noise-assisted release—that cannot appear in a purely diffusive model on the same graph and with the same sink coupling.

- CRN: trace-preserving GKSL dynamics on N hypothesis nodes with node-local dephasing rate κ and an explicit sink state $|s\rangle$ coupled to the target at rate η.
- CRW: continuous-time random walk on the same adjacency (Laplacian generator), augmented by the same target→sink absorption rate η.
- Topology: a trap-inducing "lollipop" graph (a ring attached to a tail), N = 10. This toy topology is widely used to illustrate coherent trapping: in the coherent limit $\kappa \to 0$, destructive interference can confine probability mass to a dark subspace with weak overlap to the sink; dephasing releases this trapping.
- Initial condition: localized at node 0; target node: N-1.
-

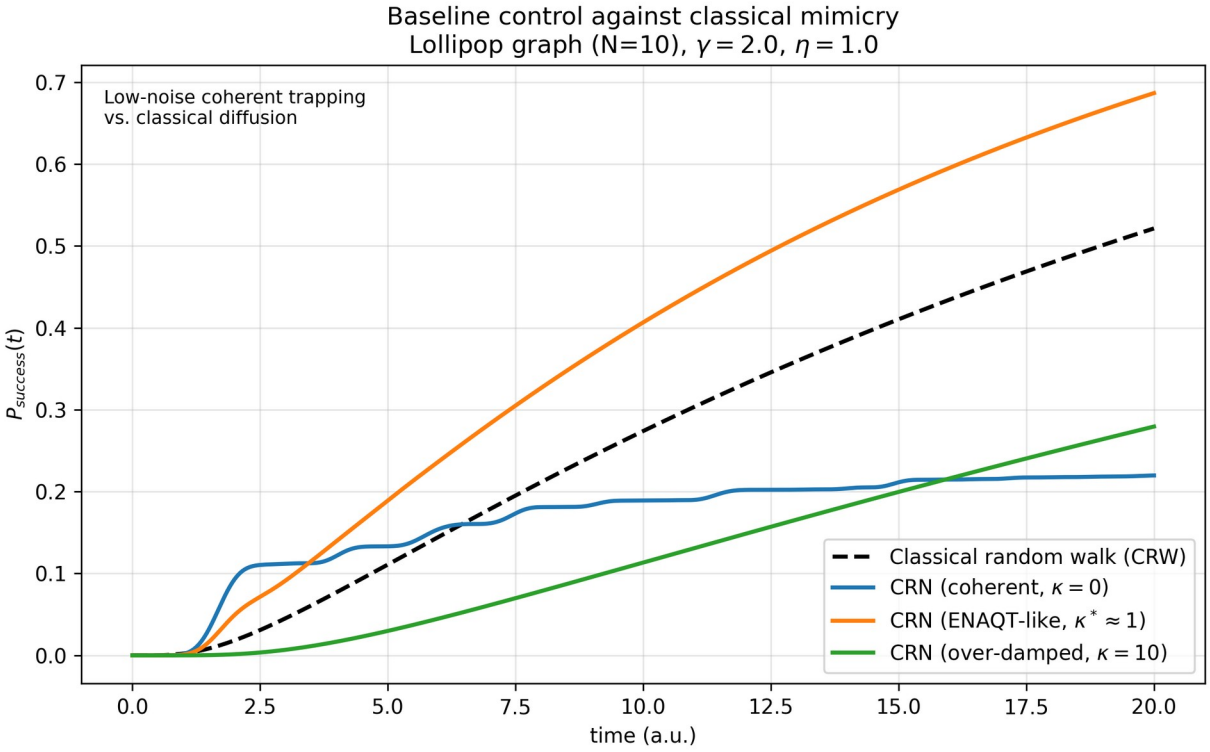

Supplementary Figure S6-1: Baseline CRN vs CRW comparison (S6_baseline_comparison.png).
Cumulative success probability P_success(t) for CRN (solid curves) versus a classical random walk baseline (dashed), on the same lollipop topology (N = 10, γ = 2.0, η = 1.0). In the coherent limit (κ = 0), CRN exhibits a rapid initial rise followed by a pronounced stall/plateau consistent with interference trapping, while CRW continues a monotonic diffusive approach. At intermediate dephasing (κ* ≈ 1, chosen by the spectral-gap optimum), CRN escapes the trapped subspace and outperforms the classical baseline over the entire simulated horizon. In the over-damped regime (κ = 10), transport slows and falls below CRW, consistent with a Zeno-like limit.

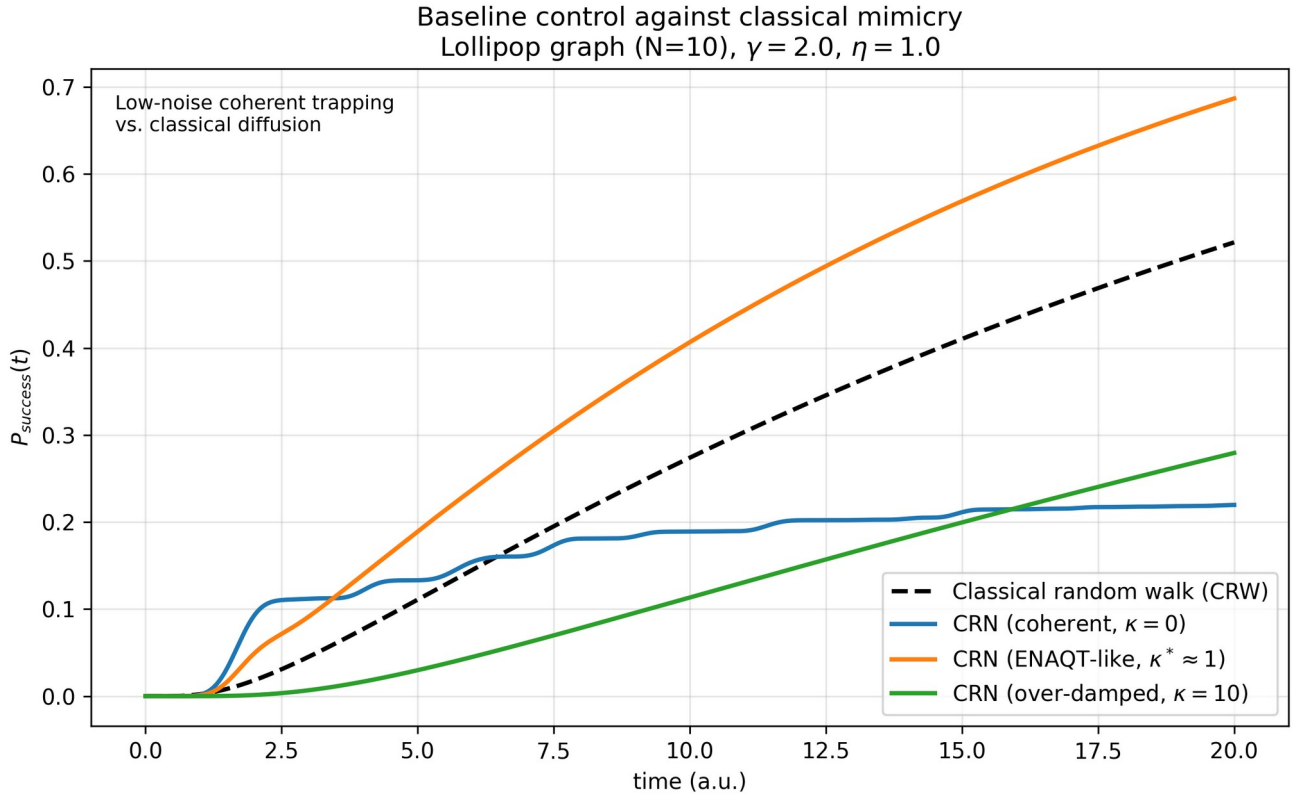

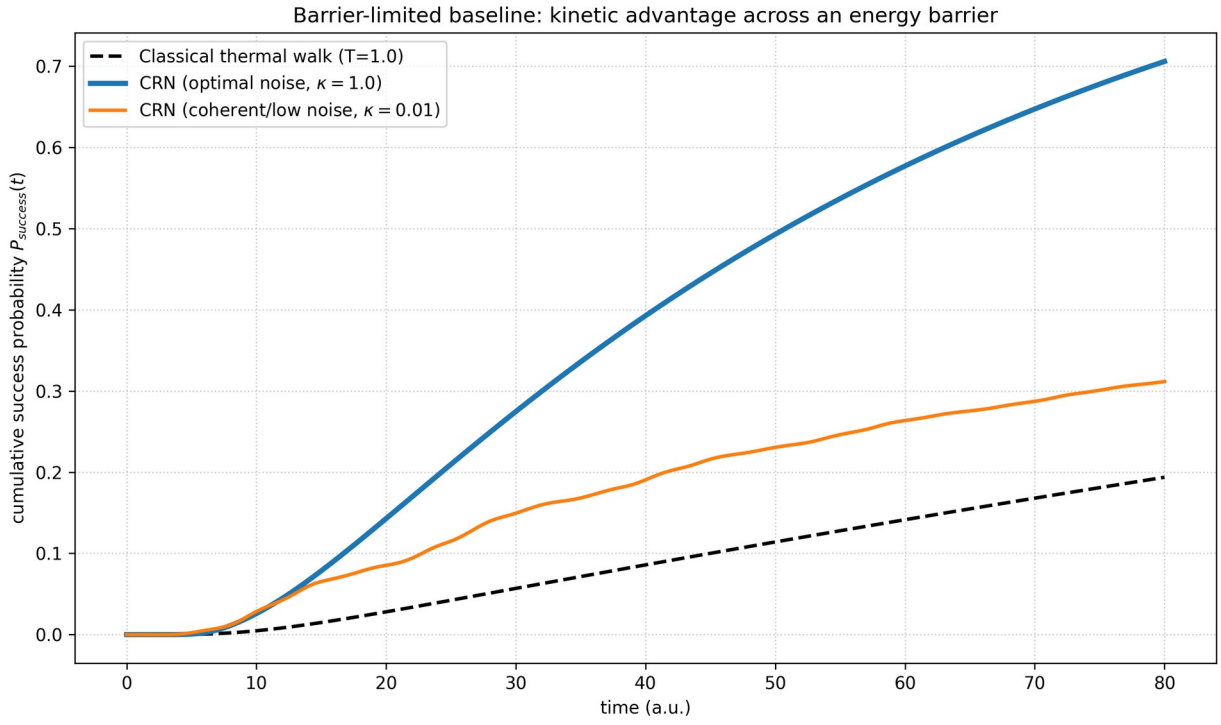

Supplementary Figure S6-2: Barrier-limited baseline (S6_barrier_crossing.png).
Additional baseline scenario on the same chain topology (N=10) with a diagonal potential barrier (V0=3 over middle nodes). The dashed curve is a classical thermal continuous-time random walk (CRW) with Arrhenius/Metropolis-like uphill suppression at fixed temperature T=1.0 and sink absorption at the target.

Solid curves are CRN (GKSL wave dynamics) with low noise (coherent limit; κ=0.01) and intermediate noise (κ=1.0), illustrating noise-assisted escape from barrier/reflection-limited transport. This panel is intended as an intuitive complement to Figure S6-1, not as an additional required falsification criterion.